

# Spectral Synthesis via Mean Field approach Independent Component Analysis

Ning Hu, Shan-Shan Su and Xu Kong

CAS Key Laboratory for Researches in Galaxies and Cosmology, Department of Astronomy,  
University of Science and Technology of China, Hefei, Anhui 230026, China  
[huning@mail.ustc.edu.cn](mailto:huning@mail.ustc.edu.cn); [xkong@ustc.edu.cn](mailto:xkong@ustc.edu.cn)

**Abstract** In this paper, we apply a new statistical analysis technique, Mean Field approach to Bayesian Independent Component Analysis (MF-ICA), on galaxy spectral analysis. This algorithm can compress the stellar spectral library into a few Independent Components (ICs), and galaxy spectrum can be reconstructed by these ICs. Comparing to other algorithms which decompose a galaxy spectrum into a combination of several simple stellar populations, MF-ICA approach offers a large improvement in the efficiency. To check the reliability of this spectral analysis method, three different methods are used: (1) parameter-recover for simulated galaxies, (2) comparison with parameters estimated by other methods, and (3) consistency test of parameters from the Sloan Digital Sky Survey galaxies. We find that our MF-ICA method not only can fit the observed galaxy spectra efficiently, but also can recover the physical parameters of galaxies accurately. We also apply our spectral analysis method to the DEEP2 spectroscopic data, and find it can provide excellent fitting for those low signal-to-noise spectra.

**Key words:** methods: data analysis – methods: statistical – galaxies: evolution – galaxies: fundamental parameters – galaxies: stellar content

## 1 INTRODUCTION

Spectrum contains plentiful information about the properties of galaxy (Kong et al., 2014). Finding a way to analyze the spectra of observed galaxies and determine the parameters of large sample of galaxies would not only help us to investigate galaxy formation and evolution, but also allow us to derive cosmological information from a large number of galaxies (Conroy, 2013). Many methods, based on the used features, were devised to measure and understand the physical parameters of galaxies, whether by using the spectral indices (Worthey et al., 1994) or emission features (Kewley et al., 2001; Shi et al., 2014), or by fitting full spectrum (Tremonti et al., 2004; Cid Fernandes et al., 2005; Ocvirk et al., 2006; Tojeiro et al., 2007; Liu et al., 2013). Due to the abundance of high-quality galaxy spectra, two different population synthesis approaches have been commonly used to study the stellar contents of galaxy. Empirical population synthesis method (Faber, 1972; Bica, 1988; Cid Fernandes et al., 2001; Kong et al., 2003) is based on modelling galaxies as mixture of several observed spectra of stars or star clusters. However, this method do not consider the stellar evolution and is limited by the observed stellar/cluster spectral library. Recently, a more direct approach so-called evolutionary population synthesis (Vazdekis, 1999; Girardi et al., 2000; Bruzual & Charlot, 2003, hereafter BC03; Maraston, 2005; Chen et al., 2015) has been widely used. In this approach, the spectra of stellar populations are modeled by combining stellar evolution tracks, SSP library and star formation histories (SFHs). Up to now, a popular simple stellar populations (SSPs) library was provided by the isochrone synthesis technique

(BC03). Several groups have selected a few SSPs from this library as templates to fit the observed galaxy spectra (Tremonti et al., 2004; Cid Fernandes et al., 2005).

However, the advent of large-area spectroscopic surveys, such as the Third Sloan Digital Sky Survey (SDSS-III; Eisenstein et al., 2011), the Deep Extragalactic Evolutionary Probe 3 (DEEP3) Galaxy Redshift Survey (Cooper et al., 2011), and the Large sky Area Multi-Object fiber Spectroscopic Telescope (LAMOST; Cui et al., 2012), will be providing oceans of data, thus the development of fast and automated extraction methods are required. We note that statistical analysis techniques have been commonly implemented. For example, Richards et al. (2009) utilized the diffusion  $k$ -means method to draw several prototype spectra from SSP database as input templates of the spectral synthesis software STARLIGHT (Cid Fernandes et al., 2005). Nolan et al. (2006) applied a data-driven Bayesian approach to the spectra of early-type galaxies. Another blind source separation (BSS) technique applied to spectra is principal component analysis (PCA, Mittaz, Penston & Sniijders 1990, Kong & Cheng 2001; Yip et al. 2004), but the interpretation of the individual component spectra seems rarely illuminating. Here, we explore a new statistical multivariate data processing technique, independent component analysis (ICA), in our spectral analysis. This technique has been implemented in the Cosmic Microwave Background studies (Maino et al., 2007) and the analysis of spectra (Lu et al., 2006; Allen et al., 2013), however, the Ensemble Learning ICA (EL-ICA, also known as naive mean field or NMF) method used in Lu et al. (2006) is known to fail in some circumstances (e.g. low signal-to-noise spectra) (Højjen-Sørensen et al., 2001), and Allen et al. (2013) applied to only emission-line galaxies. For the sake of non-negative values in the galaxy spectral analysis, we adopt a new ICA algorithm, mean field approach independent component analysis (MF-ICA), which can constrain the sources and the mixing matrix to be non-negative with a more efficient and more reliable algorithm.

The paper is structured as follows. In Section 2, we introduce the MF-ICA method, and derive a few templates from evolutionary population models of Charlot & Bruzual (2007) to analyze the spectra of galaxy. In Section 3, the simulated galaxy spectra are used to analyze the reliability of the MF-ICA method. In Section 4, we analyze the SDSS observed galaxy spectra, compare our results with those obtained from the MPA/JHU<sup>1</sup> catalogs, to investigate whether our synthesis results are reasonable. In Section 5, some galaxy spectra from the DEEP2 galaxy redshift survey are fitted by our method, and our conclusions are outlined in Section 6.

## 2 METHOD

### 2.1 Stellar Population Models

Stellar population models can be generated by several population synthesis codes, here we adopt the 2007 version of Galaxev<sup>2</sup> (Charlot & Bruzual, 2007, CB07 hereafter), which is a new version of BC03. The CB07 models have undergone a major improvement recently with the new stellar evolution prescriptions of Marigo & Girardi (2007) for the Thermally-Pulsing Asymptotic Giant Branch (TP-AGB) evolutionary phase of low- and intermediate-mass stars. An accurate modelling of this phase is related to correct predicted fluxes at the wavelength range of  $1 - 2.5\mu\text{m}$  (Charlot & Bruzual, 2007).

The CB07 models use an empirical spectral library with a range of wavelength ( $91\text{\AA} - 36000\mu\text{m}$ ,  $N = 6917$ ), and spectral resolution about  $3\text{\AA}$ . Moreover, CB07 contains a large sample of SSP, which covers 221 different ages from  $1.0 \times 10^5$  to  $2.0 \times 10^{10}$  yr, and a wide range of initial chemical compositions,  $Z = 0.0001, 0.0004, 0.004, 0.008, 0.02, 0.05$  and  $0.1$  ( $Z_{\odot} = 0.02$ ). The observed spectrum of a galaxy can be expressed as a combination of these individual SSPs with weights. This SSPs database will be used to derive our templates in Section 2.2.3.

---

<sup>1</sup> <http://www.mpa-garching.mpg.de/SDSS/>

<sup>2</sup> <http://www.bruzual.org>

## 2.2 MF-ICA technique

### 2.2.1 Independent Component Analysis (ICA)

ICA is a new multivariate data processing method which aims at decomposing complex multivariate observations to a combination of a few hidden original sources (Hyvärinen et al., 2001). Comparing to the traditional multivariate data processing methods, such as principal component analysis (PCA) or factor analysis, ICA is much powerful for finding the hidden sources, even when those traditional methods fail completely. The following generative model of ICA shows that multivariate observations or mixed signals  $x^i$ ,  $i=1, 2, \dots, m$ , are a combination of hidden sources, i.e. Independent Components,  $h_k$ ,  $k=1, 2, \dots, n$ , with additive Gaussian noise  $\Gamma^i$ , weighted by the mixing weights  $w_k^i$  ( $m \times n$ ):

$$x^i = \sum_{k=1}^n w_k^i h_k + \Gamma^i \quad (i = 1, 2, \dots, m). \quad (1)$$

In our analysis, we take the multivariate observations as the spectra of stellar systems (e.g. SSP database), and adopt the assumption that each spectrum  $f^i(\lambda)$  can be expressed as a sum of several Independent Components (ICs),  $IC_k(\lambda)$ , so the model can be written as:

$$f^i(\lambda) = \sum_{k=1}^n w_k^i IC_k(\lambda) + \Gamma^i(\lambda) \quad (2)$$

Here, we only know the spectrum  $f^i(\lambda)$ , the unknown mixing weights  $w_k^i$ , the independent components  $IC_k(\lambda)$  and the noise can be estimated from ICA algorithms, such as Joint Approximate Diagonalization of Eigenmatrices (JADE; Cadoso & Souloumiac, 1993), extended InfoMax (Bell & Sejnowski, 1995), FastICA (Hyvärinen et al., 2001), Ensemble Learning ICA (EL-ICA; Miskin & Mackay 2001), Mean Field ICA (MF-ICA; Højen-Sørensen et al., 2002) and many others.

### 2.2.2 Mean Field approach ICA (MF-ICA)

The ICA algorithm we adopt to our spectral analysis is MF-ICA method. Comparing to other algorithms, MF-ICA is a Bayesian iterative algorithm which can constraint sources and mixing matrix to be positive by offering priors of them. The main advantage of MF-ICA algorithm is its implementation simplicity and generality.

In this approach, the likelihood for the parameters and sources is defined as  $P(\mathbf{X}|\mathbf{W}, \mathbf{\Sigma}, \mathbf{H})$  given by:

$$P(\mathbf{X}|\mathbf{W}, \mathbf{\Sigma}, \mathbf{H}) = (\det 2\pi \mathbf{\Sigma})^{-\frac{n}{2}} e^{-\frac{1}{2} \text{Tr}(\mathbf{X} - \mathbf{W}\mathbf{H})^T \mathbf{\Sigma}^{-1} (\mathbf{X} - \mathbf{W}\mathbf{H})}, \quad (3)$$

where  $\mathbf{W}$  is mixing matrix,  $\mathbf{X} = [x^1, x^2, \dots, x^m]^T$  is mixed signals matrix,  $\mathbf{\Sigma}$  is noise covariance matrix,  $n$  is the number of input source signal, and  $\det$  is the determinant of the matrix. The likelihood of the parameters is defined as  $P(\mathbf{X}|\mathbf{W}, \mathbf{\Sigma})$  obtained from:

$$P(\mathbf{X}|\mathbf{W}, \mathbf{\Sigma}) = \int d\mathbf{H} P(\mathbf{X}|\mathbf{W}, \mathbf{\Sigma}, \mathbf{H}) P(\mathbf{H}). \quad (4)$$

If priors on the mixing weight  $P(\mathbf{W})$  and the sources  $P(\mathbf{H})$  are taken into account, then the posteriors of sources and mixing matrix are obtained from  $P(\mathbf{H}|\mathbf{X}, \mathbf{W}, \mathbf{\Sigma}) \propto P(\mathbf{X}|\mathbf{W}, \mathbf{\Sigma}, \mathbf{H}) P(\mathbf{H})$  and  $P(\mathbf{W}|\mathbf{X}, \mathbf{\Sigma}) \propto P(\mathbf{X}|\mathbf{W}, \mathbf{\Sigma}) P(\mathbf{W})$ , respectively. In MF-ICA method, the noise covariance  $\mathbf{\Sigma}$  and mixing matrix  $\mathbf{W}$  can be obtained from maximum a posteriori, while sources  $\mathbf{H}$  can be obtained from their posterior mean. The mean field approach can be solved by:

$$\hat{\mathbf{H}} = \langle \mathbf{H} \rangle \quad (5)$$

$$\hat{\mathbf{W}} = \mathbf{X} \langle \mathbf{H}^T \rangle \langle \mathbf{H} \mathbf{H}^T \rangle^{-1} \quad (6)$$

$$\Sigma = \frac{1}{n} \langle (\mathbf{X} - \hat{\mathbf{W}}\hat{\mathbf{H}})(\mathbf{X} - \hat{\mathbf{W}}\hat{\mathbf{H}})^T \rangle, \quad (7)$$

where  $\langle \cdot \rangle = \langle \cdot \rangle_{\mathbf{H}|\mathbf{W},\Sigma,\mathbf{X}}$  denotes the posterior average with respect to the sources given the mixing matrix and noise covariance. The solution of MF-ICA algorithm is equal to update noise covariance (Eq. 7) and mixing matrix (Eq. 6) alternatively, and estimate sources (Eq. 5). Thus the optimized matrices of mixing matrix  $\hat{\mathbf{W}}$ , noise covariance  $\Sigma$ , and sources  $\hat{\mathbf{H}}$  can be derived from this iterative method. More details about the MF-ICA method can be found in Højen-Sørensen et al. (2002) and the available MATLAB toolbox (<http://mole.imm.dtu.dk/toolbox/ica>).

Through the Bayesian inference of the mixing matrix and sources, their priors can be constrained to be non-negative, which will be useful in observed galaxy spectrum processing, since the spectra parameters should not be negative. Although EL-ICA method has been implemented in galaxy spectral analysis (Lu et al., 2006), here we adopt the MF-ICA method, which relies on advanced mean field approaches: linear response theory and an adaptive version mean-field approach. Højen-Sørensen et al. (2001, 2002) have investigated both MF-ICA and EL-ICA methods, they concluded that comparing to the EL-ICA method, the advanced mean field approaches can recover the correct sources even when the ensemble learning theory fails, and the convergence rate of MF-ICA method is found to be faster. The comparison of these two ICA methods will be described in Section 3.3.

### 2.2.3 SSPs Spectral Analysis using MF-ICA

Through the multivariate data processing technique, we expect to derive a minimal number of non-negative templates, which can represent the spectra of galaxy with minimal loss of information. Here, we adopt the MF-ICA algorithm to compress the spectral library of SSP from CB07 models (Section 2.1).

The SSP database of CB07 contains 1547 spectra (Section 2.1), each spectrum was first truncated to the high resolution wavelength range of 3322 – 9200Å, to match that of SDSS spectrograph. In EL-ICA method, the number of sources (i.e. ICs) should be same as the number of mixed signals. Therefore, Lu et al. (2006) picked up a subsample out of the BC03 SSP database as the mixed signals matrix  $\mathbf{X}$  in the EL-ICA method, and estimated 74 hidden spectra. Finally they choose several ICs from these hidden spectra by the average fractional contribution to BC03 SSP database. However, the MF-ICA method we applied can do the dimensional reduction. Here the whole CB07 SSP database was set as the input mixed signals matrix  $\mathbf{X}$ , then the MF-ICA method will be applied to them, and the output ICs will be more precise. To avoid negative values appearing in spectral analysis, we set the priors of mixing matrix and sources as positive.

As has been mentioned above, the number of ICs can be less than mixed signals number in MF-ICA method, thus it should be predefined. The correct number can be determined as follows. We apply Root-Sum-Square (RSS) method to select the proper number of ICs. The value of RSS between the original mixed signals (i.e. whole SSP database) and the recovered mixed matrix can be calculated by:

$$\text{RSS} = \left( \sum_{j=1}^n \sum_{i=1}^m (x_j^i - \hat{x}_j^i)^2 \right)^{1/2}, \quad (8)$$

where the recovered mixed matrix  $\hat{\mathbf{X}}$  is calculated from the estimated mixing matrix and sources:  $\hat{\mathbf{X}} = \hat{\mathbf{W}}\hat{\mathbf{H}}$ . We preset the initial number of sources as one, then increase the number and the value of RSS will be reduced. Repeated this process until the reduction is no longer significant. Finally, the number of ICs can be set as **12**.

Using the number of ICs we determined, the sources can be obtained from MF-ICA calculation. Therefore, the SSP database can be compressed into 12 ICs, we present these 12 ICs in Figure 4 of Su et al. (2013).

To confirm the reliability and quality of the ICs, we used the estimated 12 ICs to recover the 1547 CB07 SSP database as follows:

$$f_{\text{SSP}}^i(\lambda) = \sum_{k=1}^{12} w_k^i \text{IC}_k(\lambda) \quad (i = 1, 2, \dots, 1547), \quad (9)$$

And we found that the spectra reconstructed by these 12 ICs excellently match with the SSP database.

### 2.3 Fitting Galaxy Spectra

The aim of this study is using these estimated 12 ICs to fit galaxy spectra from large surveys. The SFHs of galaxy can be approximated as a combination of discrete bursts, thus the population of galaxy can be decomposed into SSPs combination. As shown in Section 2.2.3, the SSP database can be compressed into 12 ICs, so the model of observed galaxy spectra,  $f_g(\lambda)$ , can be fitted by these 12 ICs as:

$$f_g(\lambda) = r(\lambda) \sum_{k=1}^{12} a_k \text{IC}_k(\lambda, \sigma), \quad (10)$$

where  $r(\lambda)$  is the reddening term, describes the intrinsic starlight reddening, can be modeled by the extinction law of Charlot & Fall (2000).  $\text{IC}_k(\lambda, \sigma)$  is the  $k$ -th IC convolved with a Gaussian function. The Gaussian width  $\sigma$  corresponds to the stellar velocity dispersion of a galaxy. During the fitting process, we mask points around the prominent lines, such as Balmer lines ( $\text{H}\epsilon$ ,  $\text{H}\gamma$ ,  $\text{H}\delta$ ,  $\text{H}\beta$ ,  $\text{H}\alpha$ ) and strong forbidden lines ( $[\text{O II}]\lambda 3727$ ,  $[\text{Ne III}]\lambda 3869$ ,  $[\text{O III}]\lambda\lambda 4959, 5007$ ,  $[\text{He I}]\lambda 5876$ ,  $[\text{O I}]\lambda 6300$ ,  $[\text{N II}]\lambda\lambda 6548, 6584$ , and  $[\text{S II}]\lambda\lambda 6717, 6721$ ).

After subtracting the modeled stellar population spectrum, emission lines can be fitted with Gaussians simultaneously, similarly as Tremonti et al. (2004): the forbidden lines ( $[\text{O II}]$ ,  $[\text{O III}]$ ,  $[\text{O I}]$ ,  $[\text{N II}]$  and  $[\text{S II}]$ ) are set to have the same line width and velocity offset, likewise for Balmer lines ( $\text{H}\gamma$ ,  $\text{H}\delta$ ,  $\text{H}\beta$  and  $\text{H}\alpha$ ). By using the procedures above, the observed galaxy spectra can be quickly recovered.

## 3 RELIABILITY OF THE FITTING METHOD

### 3.1 Simulations

In this section, we analyze the simulated galaxy spectra to examine the reliability of the MF-ICA method. All simulated spectra are generated from 2007 version of BC03 stellar population synthesis code. For sake of simplicity, we parameterize each SFH of simulated galaxy in terms of an underlying continuous model superimposed with random bursts on it (Kauffmann et al., 2003). The spectral energy distribution (SED) at time  $t$  of a stellar population characterized by an exponentially declining star formation law  $\psi(t) \propto e^{-\gamma t}$  is given by:

$$F_\lambda(t) = \int_0^t \psi(t-t') S_\lambda(t', Z) dt', \quad (11)$$

where  $S_\lambda(t', Z)$  is the power radiated by an SSP of age  $t'$  and metallicity  $Z$  per unit wavelength per unit initial mass.

The added SFHs are described below:

1. The time when a galaxy begins forming stars  $t$  is distributed uniformly between 0.1 and 13.5 Gyr. Star formation timescale  $\gamma$  is uniformly distributed between 0 and 1  $\text{Gyr}^{-1}$ .
2. Random bursts occur at any time with same probability. Bursts are parameterized in terms of the fraction of stellar mass produced, which is logarithmically distributed between 0.03 and 4, and their duration can vary between 0.03 and 0.3 Gyr.

3. The metallicities  $Z$  are uniformly distributed between  $0.02 Z_{\odot}$  and  $2 Z_{\odot}$ , which represent the range of stellar metallicities inferred from the spectra of  $\sim 2 \times 10^5$  SDSS galaxies.

We apply our spectral analysis method on 500 simulated spectra over the range  $3322 - 9200 \text{\AA}$ . We also use the extinction law of Charlot & Fall (2000) to attenuate each spectrum, where the absorption optical depth  $\tau_V$  is uniformly distributed between 0 and 5. The velocity dispersion  $\sigma$  is distributed uniformly between  $50 \text{ km s}^{-1}$  and  $450 \text{ km s}^{-1}$ . Finally we added Gaussian noise with signal-to-noise ratio  $S/N = 10, 20, 30$ , respectively.

### 3.2 Results

From the fitting of simulated spectra, we expect to examine the reliability of our spectral analysis approach which based on MF-ICA algorithm. Our main parameters of interest are  $A_V$ ,  $\sigma$ ,  $t$  and  $Z$ . Following steps are used to estimate age and metallicity:

1. The pure spectrum of stellar system of a galaxy,  $f_g(\lambda)$ , can be recovered by ICs, and it also can be represented by a combination of  $N$  SSPs. Thus we can solve the equation:

$$f_g(\lambda) = \sum_{k=1}^{12} a_k \text{IC}_k(\lambda) = \sum_{j=1}^N b_j f_{\text{SSP}}^j(\lambda). \quad (12)$$

2. We adopt 60 SSPs from CB07 database include models of 15 different ages ( $t = 0.001, 0.003, 0.005, 0.01, 0.025, 0.04, 0.1, 0.2, 0.6, 0.9, 1.4, 2.5, 5, 11, 13$  Gyr) and 4 different metallicities ( $Z = 0.004, 0.008, 0.02, 0.05$ ).
3. After solving Eq. (12), the age and metallicity can be solved by:

$$\langle \log t \rangle_L = \sum_{j=1}^{60} b_j \log(t_j) \quad (13)$$

$$\log \langle Z \rangle_L = \log \sum_{j=1}^{60} b_j Z_j. \quad (14)$$

Figure 1 shows the input parameters against estimated values from simulated spectra with  $S/N = 10, 20, 30$ . Clearly, the values of starlight reddening  $A_V$  and stellar velocity dispersion  $\sigma$  are almost well recovered. The mean square errors (MSE) between recovered and input values are less than 0.20 and 7.45, respectively, as shown in Table 1.

From the above method, a galaxy spectrum can be decomposed of 60 SSPs with weights. The estimated weights  $b_j$  can reflect the fractional contributions of  $j$ -th SSP with age  $t_j$  and metallicity  $Z_j$ . Therefore, the light-weighted age and metallicity can be estimated. As shown in Figure 1 (bottom panel), the recovered and input values of  $\langle \log t \rangle_L$  have no significant difference with MSE less than 0.20. According to the age-metallicity degeneracy problem (Bressan et al., 1996), the values of  $\log \langle Z \rangle_L$  recovered by our method cannot be exactly accurate. However, we can estimate them with meaningful accuracy, the Spearman's rank correlation coefficient  $r_s$  between output and input  $\log \langle Z \rangle_L$  is about 0.70 for  $S/N = 20$ . Finally, the summary of mean square error of parameters from simulated spectra can be found in Table 1.

### 3.3 Compare to EL-ICA method

To carefully test the influence of ICA algorithms, we re-estimated the ICs by EL-ICA algorithm (Miskin & MacKay, 2001). The EL-ICA method, which also known as naive mean field ICA method, has been applied in galaxy spectrum analysis by Lu et al. (2006). Here we used the same steps as Lu et al. (2006) and also derived six ICs, we present these six ICs in Figure 2.

We use these ICs to refit the simulated spectra, the input parameters against output estimated values and the mean square error between them for simulations with  $S/N=20$  are shown in Figure 3. The dispersions of parameters derived by EL-ICA method are larger than those by our method, which were shown in Figure 1. And the mean square errors of starlight reddening, velocity dispersion, stellar age, metallicity ( $A_V$ ,  $\sigma$ ,  $\langle \log t \rangle_L$ ,  $\log \langle Z \rangle_L$ ) are 0.421, 33.841, 0.405, and 0.299 for  $S/N=20$ , respectively. These values are much larger than those of our method, as shown in Table 1. Finally, we also fit the SSP database using these ICs, the spectra recovered are not as good as those by our method. We conclude that our method which based on MF-ICA algorithm is more precise and reliable.

## 4 APPLICATION TO SDSS SPECTRA

Using our MF-ICA spectral analysis method, we fit the SDSS galaxy spectra, analyze stellar population properties of them, and measure their emission-line properties from the starlight-subtracted spectra. In this section, we compare the physical parameters obtained from stellar population analysis of continuum and measurements of emission lines. We also compare parameters estimated from our fitting technique with those derived by the MPA/JHU group. Because the aim of this section is to test whether the results from our spectral analysis method are reasonable and meaningful, we would not investigate their physics properties, such as the formation and evolution, of galaxies.

### 4.1 Data preparation

The Sloan Digital Sky Survey (SDSS; York et al., 2000) has released huge amounts of high-quality observed spectra of objects. In this work, our spectra sample were extracted from spectroscopic plates of SDSS Data Release 8 (DR8; Aihara et al., 2011). Moreover, we choose the objects which have been spectroscopically classified as galaxies. The spectra obtained from SDSS span a wavelength from  $3800\text{\AA}$  to  $9200\text{\AA}$  with mean spectral resolution  $R = \lambda/\Delta\lambda \sim 1800$ , and taken within three arcsecond diameter fibers. We finally fit about one million spectral sample of galaxies with redshift less than 1, which obtained from SDSS spectroscopic pipeline.

We use the MF-ICA method, which was described in Section 2.3, to fit the spectral sample of galaxies from SDSS. Firstly, the spectra of galaxies were corrected for the foreground Galactic extinction, using the maps of Schlegel et al. (1998). Then, they were transformed into the rest frame, with spectroscopic redshifts. The spectral fittings results give a median  $\chi^2/\text{d.o.f}$  (degree of freedom) of 1.13, nearly to excellent value of 1 as we expected. Figure 4 shows some examples of the fitting, the spectra can be well recovered by eye-inspection, which suggest that our MF-ICA spectral analysis approach works well.

### 4.2 Comparisons with the MPA/JHU database

The MPA/JHU group has provided catalogs of estimated physical parameters of SDSS galaxies publicly available on the website.<sup>3</sup> They inferred the SFHs of DR8 galaxies on the basis of CB07 models, which was similar to our researches. Here we compare our own estimated parameters, such as the emission line measurement, and stellar population properties, with those obtained from the MPA/JHU catalogs. Although we do not expect our estimated parameters that perfectly consistent with them, we analyze the relationships between these parameters to examine the accuracy and reliability of MF-ICA algorithm.

#### 4.2.1 Stellar extinction

In our fitting technique, the extinction of optical galaxy spectra is modelled as one free parameter  $A_V$ . In Figure 5a), we plot the values of  $A_V$  estimated by our method, versus those estimated by the MPA/JHU group, which adopt the same attenuation curve by Charlot & Fall (2000). Since only few galaxies with

<sup>3</sup> See [http://www.sdss3.org/dr8/spectro/spectro\\_access.php](http://www.sdss3.org/dr8/spectro/spectro_access.php)

$A_V < 0$  are found in previous research works, we constrain  $A_V$  to be positive in our analysis. Therefore, this constrains will not have significant impact on the results of our analysis.

We adopt the value of Spearman's rank correlation coefficient  $r_s$  to describe the relationship between two variables. As shown in Figure 5a), our results are well and linearly correlated to those extracted from the MPA/JHU catalogs, with  $r_s = 0.69$ . However, the extinction values  $A_V$  which obtained from the MPA/JHU database are systematically lower with our values, similar as found in Chen et al. (2012, in Figure 3f). One possible reason for this discrepancy is that we only use the optical-band spectra to estimate the stellar extinction  $A_V$ .

#### 4.2.2 Stellar mass

By using our stellar population analysis method, the light-weighted stellar mass  $\log\langle M \rangle_L$  of SDSS galaxy also can be estimated. We calculate M/L ratio by weighed-added M/L ratios of each SSP component, and then derive the stellar mass by multiplying it by luminosity. In Figure 5b), we plot our estimate stellar mass against the MPA/JHU extinction-corrected stellar mass. The results from two methods are well consistent, with  $r_s = 0.90$ . The small discrepancy is caused due to the different estimate methods. In our method, the stellar masses are obtained from the  $M/L$  ratio, which estimated through the best  $\chi^2$  model. While the MPA/JHU group estimated their  $M/L$  ratio through Bayesian inference method, which connect two indices,  $H\delta_A$  and  $D_n(4000)$ , with a model obtained from a large library of Monte Carlo realizations of galaxies with different SFHs (Kauffmann et al., 2003).

#### 4.2.3 Emission lines and nebular metallicities

In our case the emission lines were measured from starlight-subtracted spectrum. The MPA/JHU group adopted a similar method, however, they only used a single metallicity CB07 model to fit the observed continuum. We plot our estimated equivalent widths (EWs) of emission lines, such as  $H\beta$ ,  $[O\ III]\lambda 5007$ ,  $[O\ I]\lambda 6300$ ,  $H\alpha$ ,  $[N\ II]\lambda 6584$  and  $[S\ II]\lambda 6717$  versus those measured by the MPA/JHU group in Figure 6. As shown in Figure 6, our values are consistent with those measured by the MPA/JHU group, with small discrepancy. We adopt the MSE to quantify the discrepancy between them. On the whole, the MSE of all these values are less than 1, suggest that there are no significant difference. The small discrepancy appearing is due to different measurement of the synthesized spectrum, which related to different subtracted stellar absorption.

We also compared the value of nebular oxygen abundance  $12 + \log(O/H)$ , which can be obtained from the equation described in Tremonti et al. (2004). As shown in Figure 7, our estimated values of nebular oxygen abundance show a high degree of correspondence with those drawn from the MPA/JHU catalog. The value of Spearman rank coefficient is 0.99, nearly to a perfect Spearman correlation of  $r_s = 1$ , which indicates the perfect monotonic relationship.

This part is summarized as follows. We have compared estimated parameters such as the stellar extinction, stellar mass and emission line measurement with those obtained from the MPA/JHU catalogs. According to the analysis of relationships between these parameters, we conclude that MF-ICA method is reasonable and reliable.

### 4.3 Empirical relations

In this subsection, another way was used to test the accuracy of our method. The parameters estimated from the analysis of continuum were compared with those estimated by using measured emission lines. We analyze the relationships between these parameters to investigate whether our method derived results are reasonable.

### 4.3.1 Relations between Balmer features and stellar age

The value of 4000 Å break index (Balogh et al., 1999) can reflect age of galaxy. Higher  $D_n(4000)$  values relates to older, metal-rich galaxies, while lower values related to younger stellar subpopulation of galaxies. The strength of  $H\delta_A$  (Worthey & Ottaviani, 1997) is another age indicator. Strong  $H\delta_A$  absorption of galaxy reflects a burst of star formation occurred in the past 0 – 1 Gyr. Therefore, our estimated ages of galaxies should be increased with  $D_n(4000)$  values, decreased with  $H\delta_A$  values. In Figure 8a) and b), correlations between ages,  $D_n(4000)$  and  $H\delta_A$  values are shown expected relationships,  $D_n(4000) - \langle \log t \rangle_L$  trends with  $r_s = 0.85$  are strongly positive, and  $H\delta_A - \langle \log t \rangle_L$  trends with  $r_s = -0.77$  are strongly negative.

For the galaxy with emission lines,  $H\alpha$  emission-line is corresponded to the instantaneous star formation rate (SFR) of a galaxy (Kennicutt & Evans, 2012). Therefore the equivalent width (EW) of  $H\alpha$  is also an age indicator, which would be larger for younger galaxies. Figure 8c) shows that the light-weighted stellar age  $\langle \log t \rangle_L$  correlate negatively with  $EW(H\alpha)$  ( $r_s = -0.79$ ), as we expected. These relations respect that the stellar ages  $\langle \log t \rangle_L$  we obtained by our spectral synthesis are reasonable.

### 4.3.2 Stellar mass and velocity dispersion

According to the viral theorem, for constant mass surface density, the stellar mass ( $\log M_*$ ) is expected to be correlated positively with the stellar velocity dispersion ( $\log \sigma$ ). In the sample of old galaxies,  $\sigma$  is related to galaxy mass through the Faber-Jackson relation. Moreover, the stellar velocity dispersion of young, star forming galaxies is contributed from bulge and disc, thus it is related to galaxy mass through the Tully-Fisher relation. In Figure 8d), we plot our estimates of stellar mass ( $\log M_*$ ) with velocity dispersion ( $\log \sigma$ ). The  $M_* - \sigma$  relation trend strongly positive with  $r_s = 0.82$  as we expected, which suggests our synthesis results are meaningful.

We have analyzed the correlations between physical parameters obtained from stellar populations, such as stellar ages and stellar masses, with independent quantities. The strong correlations of  $\langle \log t \rangle_L - D_n(4000)$ ,  $H\delta_A$ ,  $EW(H\alpha)$ , and  $M_* - \sigma$  suggest that the parameters derived by our spectral synthesis approach through MF-ICA method are reasonable and meaningful.

## 5 APPLICATION TO SPECTRA OF GALAXIES WITH HIGHER REDSHIFT

Optical galaxy redshift surveys are not only vital importance in cosmology, but also very important to understand physical processes related to galaxy formation and/or evolution (Fang et al., 2015). In the last few years, redshift surveys, such as 2dF Galaxy Redshift Survey (2dFGRS; Colless et al., 2001) and SDSS, have measured redshifts of millions of low redshift (with median redshift of  $z = 0.1$ ) galaxies. With larger aperture telescope, new generation redshift surveys, such as the DEEP2, BigBOSS, LAMOST, will measure redshifts of galaxies with higher redshift (Davis et al., 2007; Schlegel et al., 2009; Kong & Su, 2010; Zou et al., 2011). The motivation for this work is that we want to provide an easy-to-use full-spectrum fitting package and determine spectral parameters for spectra of the LAMOST extragalactic surveys (Kong & Su, 2010). Since the regular spectroscopic survey of LAMOST just beginning, we apply our synthesis approach to the spectra of galaxy from the DEEP2 survey, which has a similar signal-to-noise ratio as the spectrum of LAMOST (Luo et al., 2015).

In the Extended Groth Strip (EGS) field, utilizing the DEIMOS (Deep Imaging Multi-object spectrograph) boarded on the Keck 10 m telescope, DEEP2 galaxy redshift survey provides the spectral data of galaxies with the redshift from 0 to 1.4. DEIMOS have highest-revolution grating, 1200 line  $\text{mm}^{-1}$ , typically covering 6500 – 9100 Å, with a spectral resolution  $R = \lambda/\Delta\lambda \sim 6000$  (Faber et al., 2003). In our study, we only analyze galaxies with redshift quality  $Q \geq 3$ . Thus, we obtained 9501 galaxies with  $Q \geq 3$  in the EGS, corresponding to the median redshift is 0.74. The details of these galaxies spectra extraction can be found in Davis et al. (2007). Finally, we obtained about 1,400 sources with  $S/N > 3$ , and show some examples of the fitting in Figure 9. It can be seen that our MF-ICA fitting method work well, and we will analysis their physical properties in the future work.

## 6 SUMMARY

In this work, we have presented the MF-ICA method to compress the CB07 SSP library into a few Independent Components (ICs) as templates to fit observed galaxy spectra. Although there are many statistical multivariate data processing techniques, MF-ICA seems to be more useful. Since it has the capability of providing good estimates of the results by selecting proper parameters. The goal of our project was to estimate physical properties quickly and accurately for a large sample of galaxies. By using MF-ICA algorithm, we can fit an observed spectrum of galaxy only a few second, which is time-efficient for analysis of galaxies spectra observed by large-area surveys, such as LAMOST, BigBOSS.

We have tested our method to fit the simulated and the SDSS DR8 galaxy spectra. Simulations show that the important parameters of galaxies can be accurately recovered by our method, such as stellar contents, star formation histories, starlight reddening and stellar velocity dispersion.

We have compared parameters estimated from our fitting technique to those obtained from the MPA/JHU group of DR8 galaxies. These physical parameters and measurements are in good agreement. We also analyze the correlations between physical parameters obtained from stellar populations with independent quantities. We find strong correlations of  $M_* - \sigma$ ,  $\langle \log t \rangle_L - D_n(4000)$ ,  $H\delta_A$ ,  $EW(H\alpha)$ .

In future studies, we intent to apply our fitting technique to other large data bases, such as the LAMOST ExtraGalactic Surveys (LEGAS), the DEEP2 galaxy redshift survey. We have fitted more than 1,400 DEEP2 galaxies spectra, our next step will analysis their physical properties.

## ACKNOWLEDGMENTS

We are grateful to the anonymous referee for making constructive suggestions to improve the paper. We thank Stephane Charlot for providing the unpublished CB07 stellar population synthesis models and helpful discussions. This work is supported by the National Natural Science Foundation of China (NSFC, Nos. 11225315, 1320101002, 11433005, and 11421303), the Strategic Priority Research Program "The Emergence of Cosmological Structures" of the Chinese Academy of Sciences (No. XDB09000000), the Specialized Research Fund for the Doctoral Program of Higher Education (SRFDP, No. 20123402110037), and the Chinese National 973 Fundamental Science Programs (973 program) (2015CB857004).

## References

- Aihara, H., Allende Prieto, C., An, D., et al. 2011, *ApJS*, 193, 29  
 Allen J. T., Hewett P. C., Richardson C. T., Ferland G. J., Baldwin J. A., 2013, *MNRAS*, 430, 3510  
 Balogh, M. L., Morris, S. L., Yee, H. K. C., Carlberg, R. G., & Ellingson, E. 1999, *ApJ*, 527, 54  
 Bell, A. J. & Sejnowski, T. J. 1995, *Neural Comput.* 7, 1129  
 Bica, E. 1988, *A&A*, 195, 76  
 Bressan, A., Chiosi, C. & Tantolo, R. 1996, *A&A*, 311, 425  
 Bruzual, A. G. & Charlot, S. 2003, *MNRAS*, 344, 1000  
 Cadoso, J. E. & Souloumiac, A. 1993, *IEE Proc. :F Radar Signal Rrocess.*, 140, 362  
 Charlot, S. & Bruzual, A. G. 2007, in preparation  
 Charlot, S. & Fall, S. M. 2000, *ApJ*, 539, 718  
 Chen, Y., Bressan, A., Girardi, L., et al. 2015, *MNRAS*, 452, 1068  
 Chen, Y. M., Kauffmann, G., Tremonti, C. A., et al. 2012, *MNRAS*, 421, 314  
 Cid Fernandes, R., Mateus, A., Sodré, L., et al. 2005, *MNRAS*, 358, 363  
 Cid Fernandes, R., Sodré, L., Schmitt, H. R. & Leão, J. R. S. 2001, *MNRAS*, 325, 60  
 Colless, M., Dalton, G., Maddox, S., et al. 2001, *MNRAS*, 328, 1039  
 Conroy, C. 2013, *ARA&A*, 51, 393  
 Cooper, M. C., Aird, J. A., Coil, A. L., et al. 2011, *ApJS*, 193, 14  
 Cui, X. Q., Zhao, Y. H., Chu, Y. Q., et al. 2012, *Research in Astron. Astrophys. (RAA)*, 12, 1197  
 Davis, M., Guhathakurta, P., Konidaris, N. P., et al. 2007, *ApJ*, 660, 1

- Eisenstein, D. J., Weinberg, D. H., Agol, E., et al. 2011, *AJ*, 142, 72
- Faber, S. M. 1972, *A&A*, 20, 361
- Faber, S. M., Phillips, A. C., Kibrick, R. I., et al. 2003, *Proc. SPIE*, 4841, 1657
- Fang, G.-W., Ma, Z.-Y., Chen, Y., & Kong, X. 2015, *Research in Astron. Astrophys. (RAA)*, 15, 819
- Girardi, L., Bressan, A., Bertelli, G. & Chiosi, C. 2000, *A&AS*, 141, 371
- Højjen-Sørensen, P. A. D. F. R., Winther, O. & Hansen, L. K. 2001, *Advances in Neural Information Processing Systems*, Vol. 13, MIT Press, Cambridge, MA, 542
- Højjen-Sørensen, P. A. D. F. R., Winther, O. & Hansen, L. K. 2002, *Neural Comput*, 14, 889
- Hyvärinen, A., Karhunen, J. & Oja, E. 2001, *Independent Component Analysis*, John Wiley & Sons, New York, 504
- Kauffmann, G., Heckman, T. M., White, Simon D. M., et al. 2003, *MNRAS*, 341, 33
- Kennicutt, R. C., & Evans, N. J. 2012, *ARA&A*, 50, 531
- Kewley, L. J., Dopita, M. A., Sutherland, R. S., et al. 2001, *ApJ*, 556, 121
- Kong, X., Charlot, S., Weiss, A., & Cheng, F. Z. 2003, *A&A*, 403, 877
- Kong, X., & Cheng, F. Z. 2001, *MNRAS*, 323, 1035
- Kong, X., Lin, L., Li, J.-r., et al. 2014, *ChA&A*, 38, 427
- Kong, X., & Su, S. 2010, *IAU Symposium*, 262, 295
- Liu, G., Lu, Y., Chen, X., Du, W., & Zhao, Y. 2013, *Research in Astron. Astrophys. (RAA)*, 13, 1025
- Lu, H., Zhou, H., Wang, J., et al. 2006, *AJ*, 131, 790
- Luo, A.-L., Zhao, Y.-H., Zhao, G., et al. 2015, *Research in Astron. Astrophys. (RAA)*, 15, 1095
- Maino, D., Donzelli, S., Banday, A. J., Stivoli, F. & Baccigalupi, C. 2007, *MNRAS*, 374, 1207
- Marigo, P. & Girardi, L. 2007, *A&A*, 469, 239
- Maraston, C. 2005, *MNRAS*, 362, 799
- Miskin, J. W. & MacKay, D. J. C. 2001, in *Independent Component Analysis: Principles and Practice*, Edited by Roberts, S. & Everson R.
- Mittaz J. P. D., Penston M. V., Snijders M. A. J., 1990, *MNRAS*, 242, 370
- Nolan, L. A., Harva, M. O., Kabán, A. & Raychaudhury, S. 2006, *MNRAS*, 366, 321
- Ocvirk, P., Pichon, C., Lançon, A. & Thiébaud, E. 2006, *MNRAS*, 365, 46
- Richards, J. W., Freeman, P. E., Lee, A. B. & Schafer, C. M. 2009, *MNRAS*, 399, 1044
- Schlegel, D. J., Finkbeiner, D. P., & Davis, M. 1998, *ApJ*, 500, 525
- Schlegel, D. J., Bebek, C., Heetderks, H., et al. 2009, arXiv:0904.0468
- Shi, F., Liu, Y.-Y., Kong, X., et al. 2014, *MNRAS*, 444, L49
- Su, S., Kong, X., Li, J., & Fang, G. 2013, *ApJ*, 778, 10
- Tojeiro R., Heavens A. F., Jimenez R., Panter B., 2007, *MNRAS*, 381, 1252
- Tremonti C. A., Heckman, T. M., Kauffmann, G., et al. 2004, *ApJ*, 613, 898
- Vazdekis, A. 1999, *ApJ*, 513, 224
- Worthey, G., Faber, S. M., Gonzalez, J. J. & Burstein, D. 1994, *ApJS*, 94, 687
- Worthey, G. & Ottaviani, D. L. 1997, *ApJS*, 111, 377
- Yip C. et al., 2004, *AJ*, 128, 585
- York, D. G., Adelman, J., Anderson, J. E., et al. 2000, *AJ*, 120, 1579
- Zou, H., Yang, Y.-B., Zhang, T.-M., et al. 2011, *Research in Astron. Astrophys. (RAA)*, 11, 1093

**Table 1** Summary of Parameter Error Estimates for Simulated Spectra. The different rows list the mean square error (MSE) between output and input values of the corresponding quantity, as obtained from simulations with different signal-to-noise ratios (S/N).

S/N	MSE <sub>A<sub>V</sub></sub> (mag)	MSE <sub>σ</sub> (km s <sup>-1</sup> )	MSE <sub>(log t)<sub>T</sub></sub>	MSE <sub>log(Z)<sub>T</sub></sub>
10	0.191	7.449	0.201	0.201
20	0.169	6.301	0.189	0.202
30	0.119	6.017	0.169	0.196

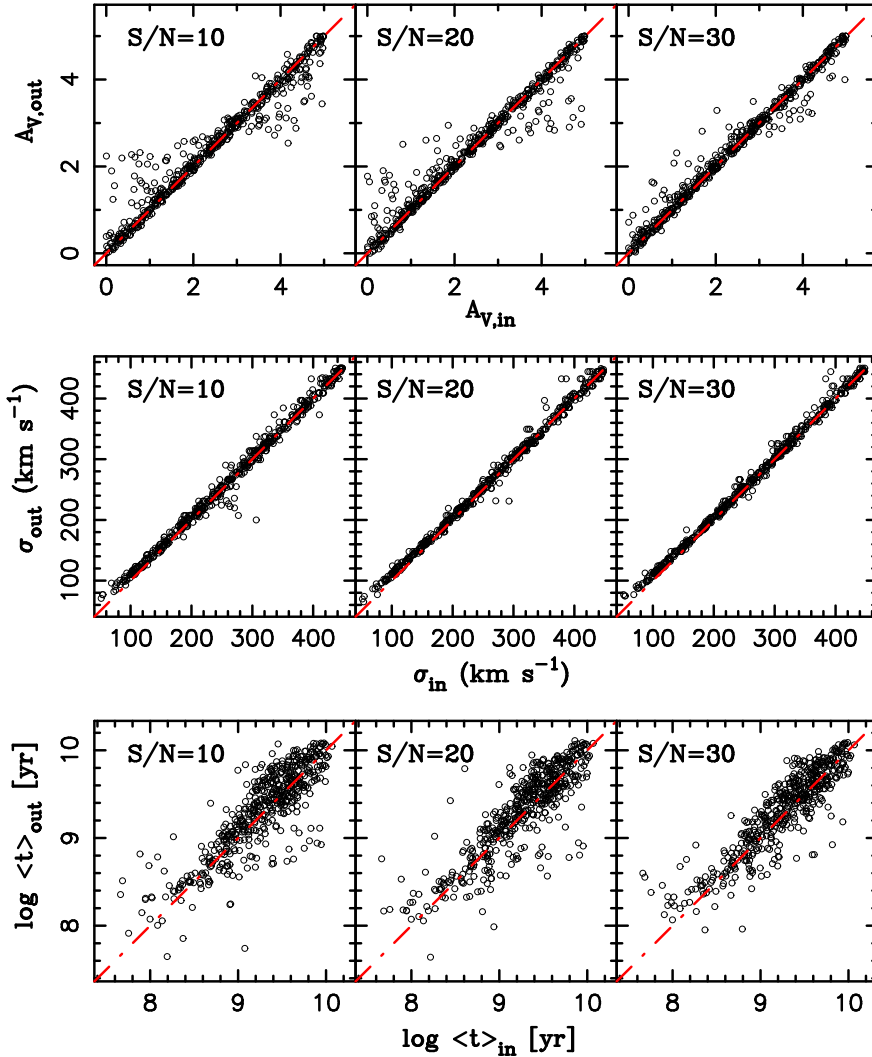


**Fig. 1** Comparison of the input  $A_V$  (magnitude),  $\sigma$  (km s<sup>-1</sup>) and stellar ages (yr) with the output estimated values for simulations, with S/N=10, 20 and 30, using our MF-ICA method. The red dot-dashed line is the identity line ( $y = x$ ).

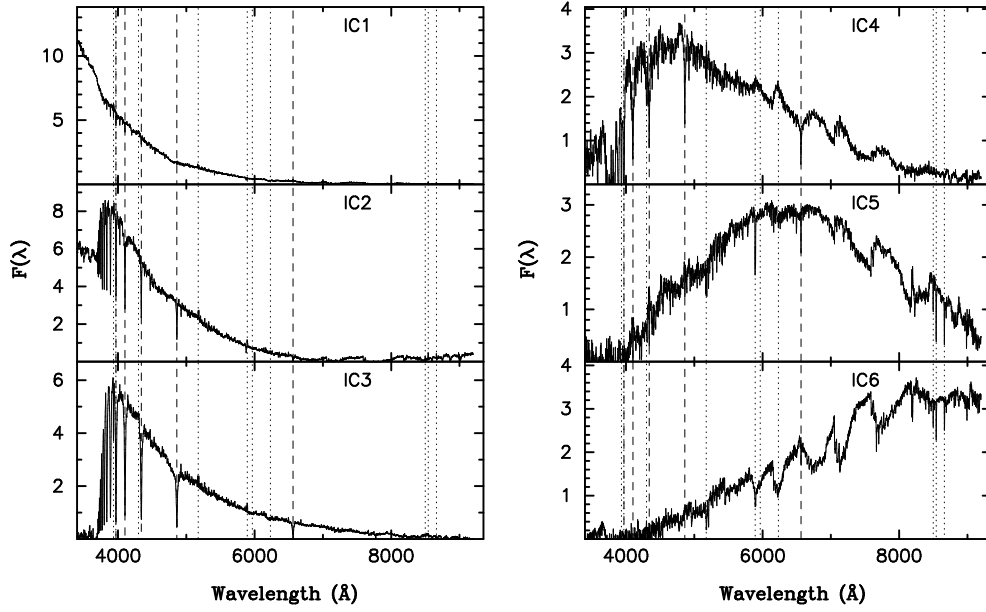


**Fig. 2** The spectra of 6 ICs estimated by EL-ICA method, some prominent spectral features are labeled same as Figure 4 in Su et al. (2013)

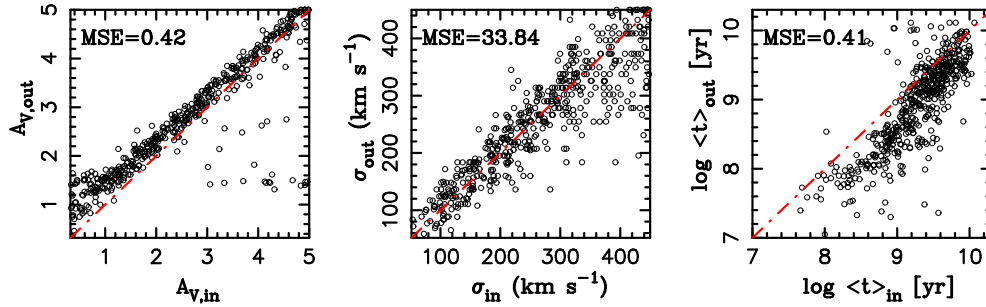


**Fig. 3** Comparison of the input  $A_V$  (magnitude),  $\sigma$  ( $\text{km s}^{-1}$ ) and stellar ages (yr) with the output estimated values for simulations, with  $S/N=20$ , using the EL-ICA method. The red dot-dashed line is the identity line ( $y = x$ ).

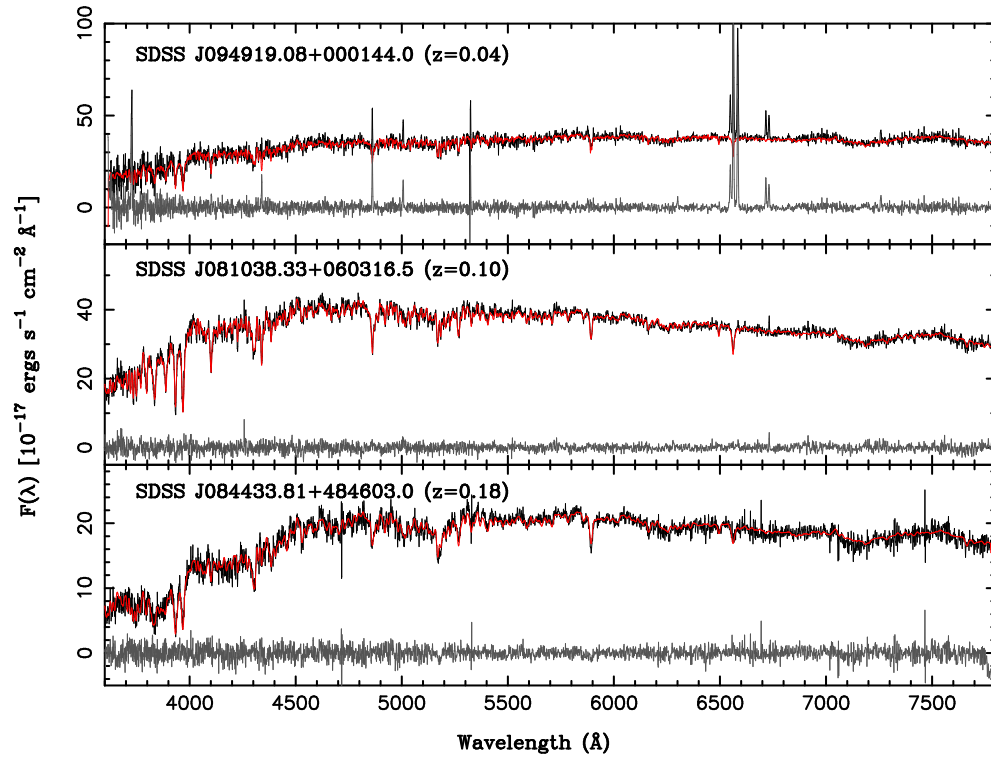


**Fig. 4** The spectra fitting results of some galaxies in our SDSS DR8 sample at a range of redshifts. The black line shows the observed spectrum, red line shows the modelled stellar spectrum, grey line shows the residual spectrum, and the redshift is labeled in the top left corner of each panel.

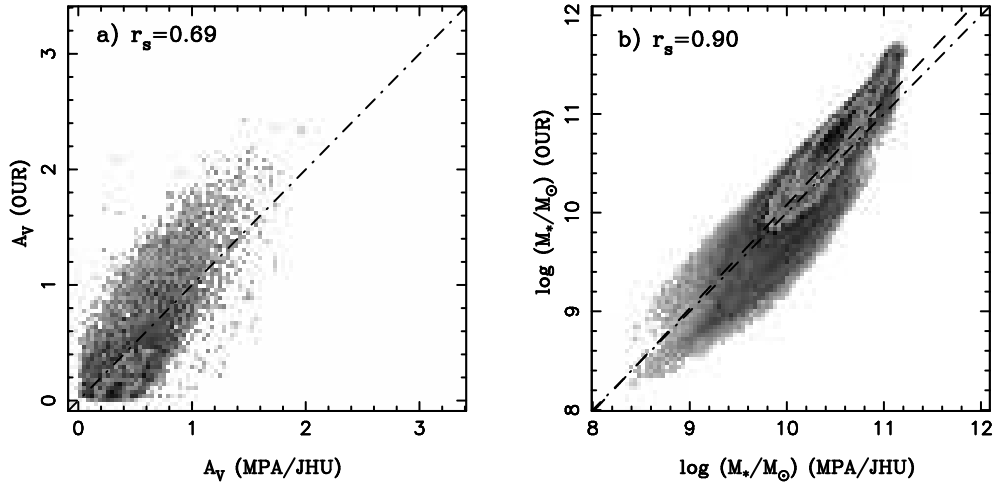


**Fig. 5** The values of stellar extinction  $A_V$  and stellar mass  $M_*$  computed from the MPA/JHU database versus those values computed by our code. The dot-dashed line is the identity line ( $y = x$ ). The dashed line in the right panel is a robust fit for the relation. The number in the top left corner is the Spearman rank correlation coefficient.

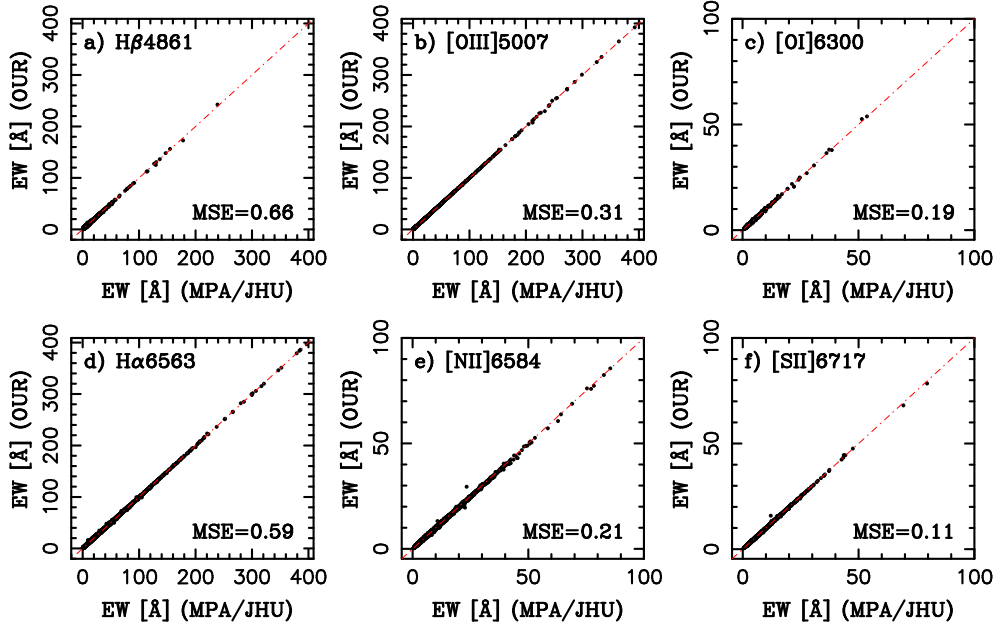


**Fig. 6** The comparison of equivalent widths of  $H\beta$ ,  $[O\text{ III}]\lambda 5007$ ,  $[O\text{ I}]\lambda 6300$ ,  $H\alpha$ ,  $[N\text{ II}]\lambda 6584$  and  $[S\text{ II}]\lambda 6717$  measured by the MPA/JHU group with those by our code. The red dot-dashed line is the identity line ( $y = x$ ), while the number in the bottom-right corner of each panel indicates the mean square error (MSE).

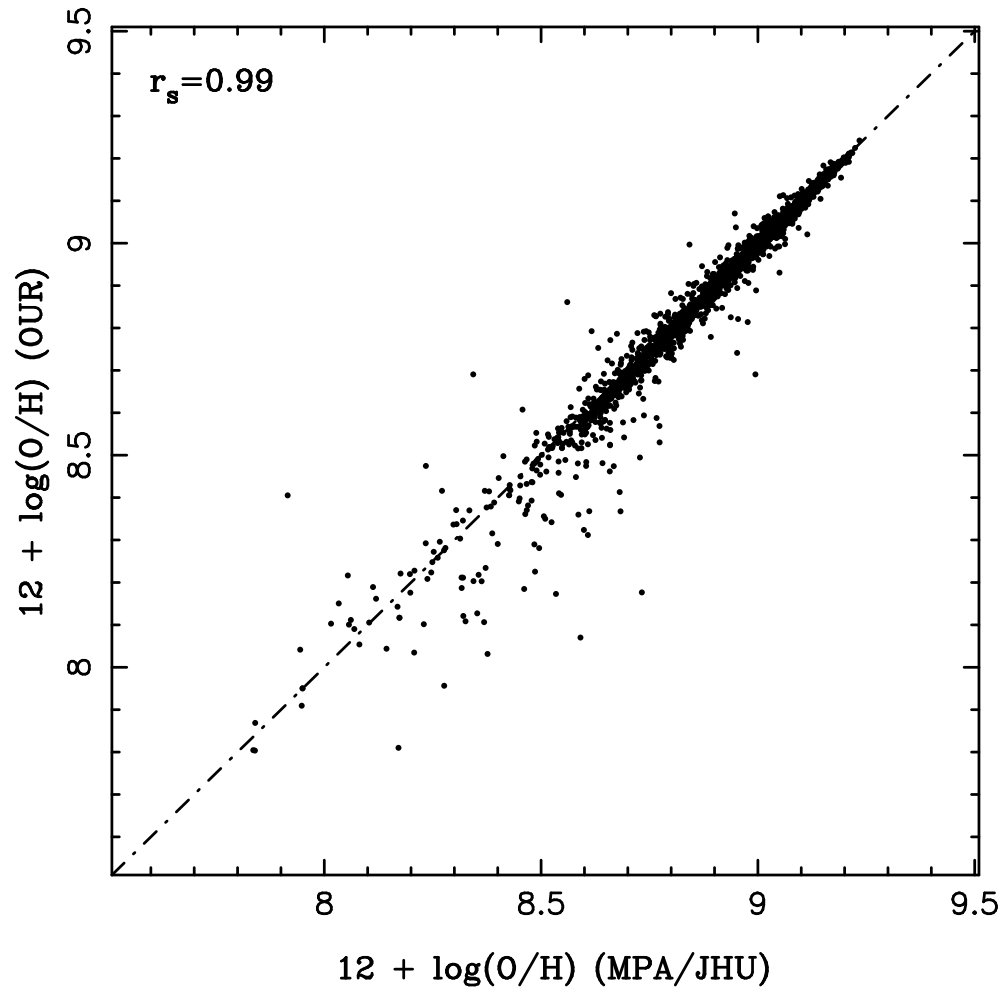


**Fig. 7** Plot of our estimated nebular oxygen abundance against those obtained by the MPA/JHU group. The dot-dashed line is the identity line ( $y = x$ ), while the number in the top left corner is the Spearman rank correlation coefficient.

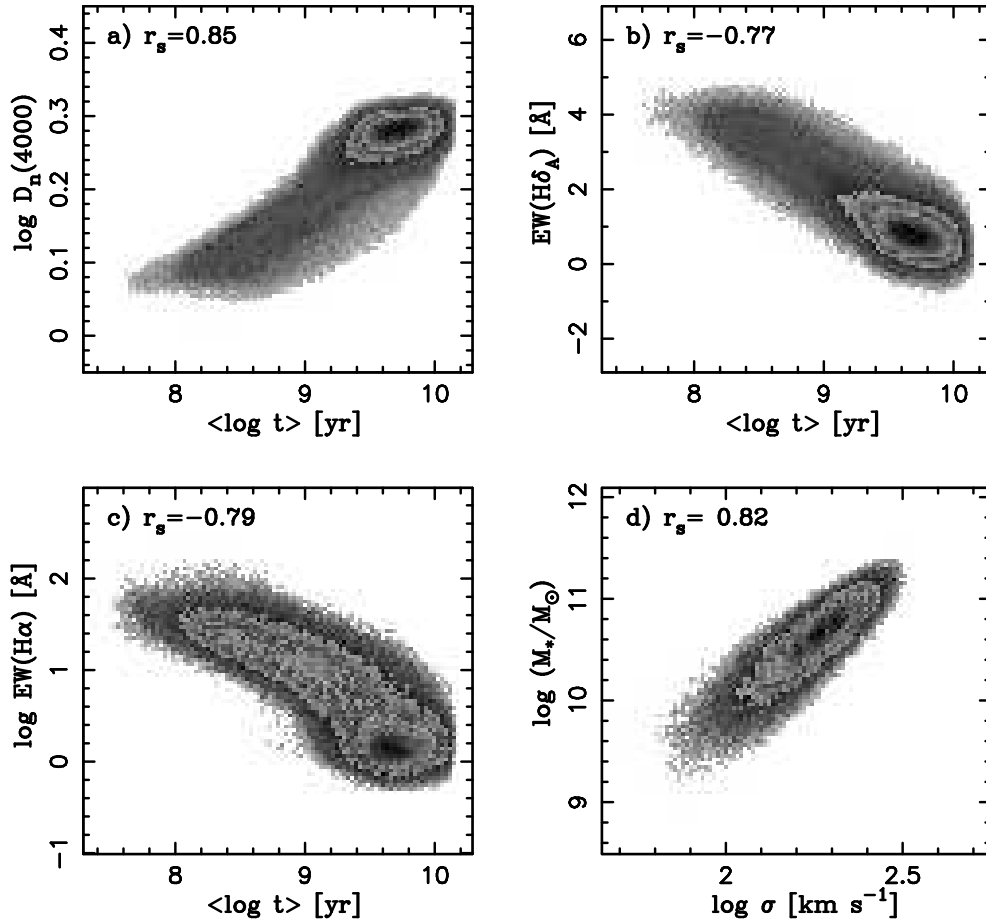


**Fig. 8** Relations of the 4000Å break index versus the light-weighted mean stellar age (a); the  $H\delta_A$  index versus the light-weighted mean stellar age (b); the equivalent width of  $H\alpha$  versus the light-weighted mean stellar age (c); the comparison of our estimated stellar mass ( $\log M_*$ ) with velocity dispersion ( $\log \sigma$ ) (d). The number in the top left corner of each panel is the Spearman rank correlation coefficient  $r_s$ .

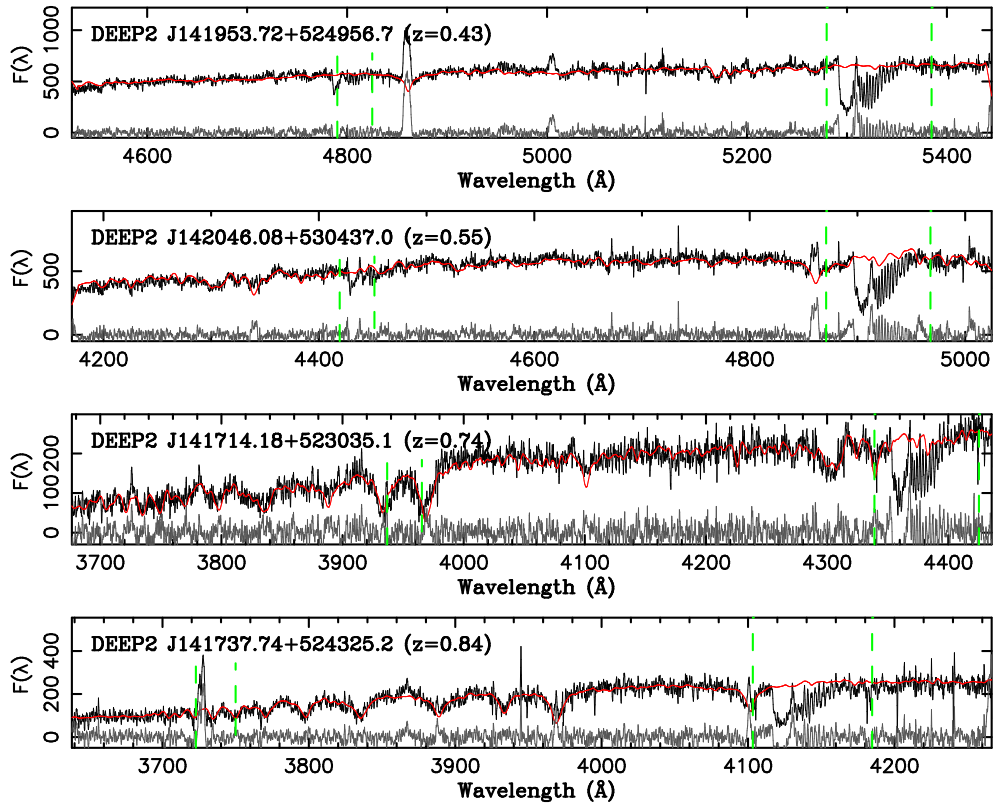


**Fig. 9** The spectra fitting results of some galaxies in our DEEP2 sample at a range of redshifts, which are labeled in the top left corner of each panel. The black line shows the observed spectrum, red line shows the modelled stellar spectrum, and grey line shows the residual spectrum. We also mask the “telluric absorption” regions between dashed lines (observed frame: 7750 – 7700  $\text{\AA}$  & 6850 – 6900  $\text{\AA}$ ).